

Surface radiation climatology for Ny-Ålesund, Svalbard (78.9° N), basic observations for trend detection

Marion Maturilli · Andreas Herber · Gert König-Langlo

Received: 15 January 2014 / Accepted: 29 April 2014

© The Author(s) 2014. This article is published with open access at Springerlink.com

Abstract At Ny-Ålesund (78.9° N), Svalbard, surface radiation measurements of up- and downward short- and longwave radiation are operated since August 1992 in the frame of the Baseline Surface Radiation Network (BSRN), complemented with surface and upper air meteorology since August 1993. The long-term observations are the base for a climatological presentation of the surface radiation data. Over the 21-year observation period, ongoing changes in the Arctic climate system are reflected. Particularly, the observations indicate a strong seasonality of surface warming and related changes in different radiation parameters. The annual mean temperature at Ny-Ålesund has risen by $+1.3 \pm 0.7$ K per decade, with a maximum seasonal increase during the winter months of $+3.1 \pm 2.6$ K per decade. At the same time, winter is also the season with the largest long-term changes in radiation, featuring an increase of $+15.6 \pm 11.6$ Wm^{-2} per decade in the downward longwave radiation. Furthermore, changes in the reflected solar radiation during the months of snow melt indicate an earlier onset of the warm season by about 1 week compared to the beginning of the observations. The supplementary dataset of Ny-Ålesund surface radiation measurements (available at <http://dx.doi.org/10.1594/PANGAEA.150000>) provides a valuable data source for the validation of satellite instruments and climate models.

1 Introduction

The Arctic is considered to be most sensitive to climate change, with warming in the Arctic occurring considerably faster than the global average (IPCC 2007). Several positive feedback mechanisms contribute to this “Arctic amplification.” A well-known concept is the snow/sea ice–albedo feedback (Curry et al. 1995; Lindsay and Zhang 2005; Screen and Simmonds 2010) which gains importance as climatic warming has caused a substantial decrease in the extent and thickness of Arctic sea ice (Cavalieri and Parkinson 2012; IPCC 2013). Also changes in atmospheric circulation and the related increase in meridional heat transport to the high latitudes account for Arctic warming (Graversen et al. 2008; Zhang et al. 2008), as well as the possibility that Arctic atmospheric circulation itself is modified by the strong warming (Francis et al. 2009; Overland and Wang 2010). Furthermore, clouds, water vapor, and their radiative feedbacks are recognized as important issues in the Arctic climate system (Curry et al. 1996; Francis and Hunter 2007), and atmospheric circulation changes augment the meridional transport of water vapor to the Arctic (Doyle et al. 2011). Stratospheric water vapor, ozone, and other greenhouse gases contribute with chemical and dynamical feedbacks in the coupled system on the global scale (e.g., Garcia and Randel 2008; Dessler et al. 2013).

All of these processes impacting Arctic climate are important concerning local feedbacks with the underlying surface but also global feedbacks on the energy balance of the planet. Altogether, radiative fluxes play a key role in the complex Arctic region. Therefore, it is necessary to have reliable long-term measurements of the surface radiation budget with the highest data quality. The Baseline Surface Radiation Network (BSRN) provides quality-controlled surface measurements of solar and terrestrial radiation with high accuracy and temporal resolution, suitable for the validation of satellite instruments

M. Maturilli (✉)

Alfred Wegener Institute, Helmholtz Centre for Polar and Marine Research, Telegrafenberg A43, 14473 Potsdam, Germany
e-mail: marion.maturilli@awi.de

A. Herber · G. König-Langlo

Alfred Wegener Institute, Helmholtz Centre for Polar and Marine Research, Am Handelshafen 12, 27570 Bremerhaven, Germany

and climate models (Ohmura et al. 1998). At the Arctic site Ny-Ålesund (78.9° N, 11.9° E), surface radiation measurements are performed by the Alfred Wegener Institute for Polar and Marine Research (AWI), contributing to the BSRN since 1 August 1992. Here, we present a thorough description of the Ny-Ålesund surface radiation data set in terms of climatology and long-term changes for the 21-year period until 31 July 2013, including August 2013 for seasonality analyses. The seasonality of surface air warming and its link to the observed changes in different radiation parameters is discussed, pointing out changes in the snow-cover period of the Ny-Ålesund environment.

2 Instrumentation

Situated at a fjord at the west coast of Svalbard (Spitsbergen), the settlement of Ny-Ålesund is a base for international Arctic research activities. The mountains towards the south determine the length of the potential sunlit period at the observation site. Generally, polar night (polar day) conditions are given between 24 October and 18 February (18 April and 24 August), respectively. Due to the orography, direct sunlight reaches Ny-Ålesund only between 8 March and 8 October.

The set-up of surface radiation observations includes direct solar radiation by pyrhelimeter, diffuse, global and reflected shortwave radiation by pyranometers, as well as up- and downward longwave radiation by pyrgeometers. All sensors used for the different radiation measurements are listed in Table 1. The according instrument for each individual measurement is indicated in the referenced dataset doi: [10.1594/PANGAEA.150000](https://doi.org/10.1594/PANGAEA.150000). As for long-term radiation measurement time series, the maintenance of the instrument calibration is critical (Dutton et al. 2006), all sensors are available twofold and exchanged on an annual/biennial basis for calibration purposes to meet the quality standard of the BSRN. While in earlier years, calibration was done at the Meteorological Observatory of the German Weather Service in Hamburg and later in Potsdam, Germany, the instruments are sent to Physikalisch-Meteorologisches Observatorium Davos/World Radiation Center (PMOD/WRC, Davos, Switzerland) since 2000. All instruments are thus traceable to the World Radiometric Reference (WRR) standards for solar radiation data and to the World Infrared Standard group (WISG) for infrared radiation. While the instrumentation has been kept stable for 19 years, the sensor type for diffuse, global, and reflected solar radiation has been changed from CM11 to CMP22 (both Kipp & Zonen products) on 22/23 August 2011, when the whole set-up has also been switched to a new data logging system. Parallel measurements of the two sensor types under polar conditions at the German Neumayer station in Antarctica lead to the conclusion that homogeneity of the long-term radiation measurements is not affected by the

sensor change. Of course, the new CMP22 sensors have been calibrated before set-up in Ny-Ålesund.

The instrumentation is regularly maintained by the AWI observatory personnel at least once per day. Disturbances by rime formation have been successfully eliminated by the installation of a specifically designed ventilation system to all affected sensors. The surface radiation measurement set-up, data retrieval, and quality control follow BSRN standards according to, e.g., McArthur (2005) and König-Langlo et al. (2013), and references therein. The high quality of the Ny-Ålesund BSRN radiation data has been documented and evaluated for the period of the International Polar Year 2007/2008 (Lanconelli et al. 2011).

The Ny-Ålesund BSRN radiation data are complemented with basic meteorological surface data for pressure, temperature, and humidity since August 1993 (Kupfer et al. 2006). More extensive meteorological auxiliary data (Maturilli et al. 2013) and additional radiation data are available online at <http://dx.doi.org/10.1594/PANGAEA.793046>. A common feature of all described radiation and meteorological parameters is the adjustment of the data registration time interval from 5- to 1-min steps that was introduced on 14 July 1998 with a renewal of the data acquisition hardware

The instrumentation for both radiation and meteorological surface measurements is located on a measurement field south of the village Ny-Ålesund. The terrain is made of soft tundra ground, covered by snow during the cold periods. The closest buildings are located about 200 m north of the radiation measurement set-up, while mountains are situated to the south. The according horizontal line is available online (<http://dx.doi.org/10.1594/PANGAEA.669522>). As the measurement site is embedded in a complex orography of mountains and fjord, local effects may cause a bias to observations in other parts of Svalbard.

3 Climatology of surface radiation parameters

Located at 78.9° N, the Ny-Ålesund radiation environment is effected by the Earth's axial tilt, characterized by the absence of solar radiation during polar night. Shortwave radiation is thus detected only during the sunlit period. Figure 1 shows the monthly mean values of all radiation parameters contributing to the net radiation budget Q_{net} that is defined as

$$Q_{net} = (SW_{down} - SW_{up}) + (LW_{down} - LW_{up})$$

with Q_{net} = net radiation budget, SW_{down} = downward (or global) shortwave radiation, SW_{up} = upward (or reflected) shortwave radiation, LW_{down} = downward longwave radiation, and LW_{up} = upward longwave radiation. In this study, monthly mean values are calculated from daily mean

Table 1 Instrumentation for long- and shortwave surface radiation used for the Ny-Ålesund BSRN measurements

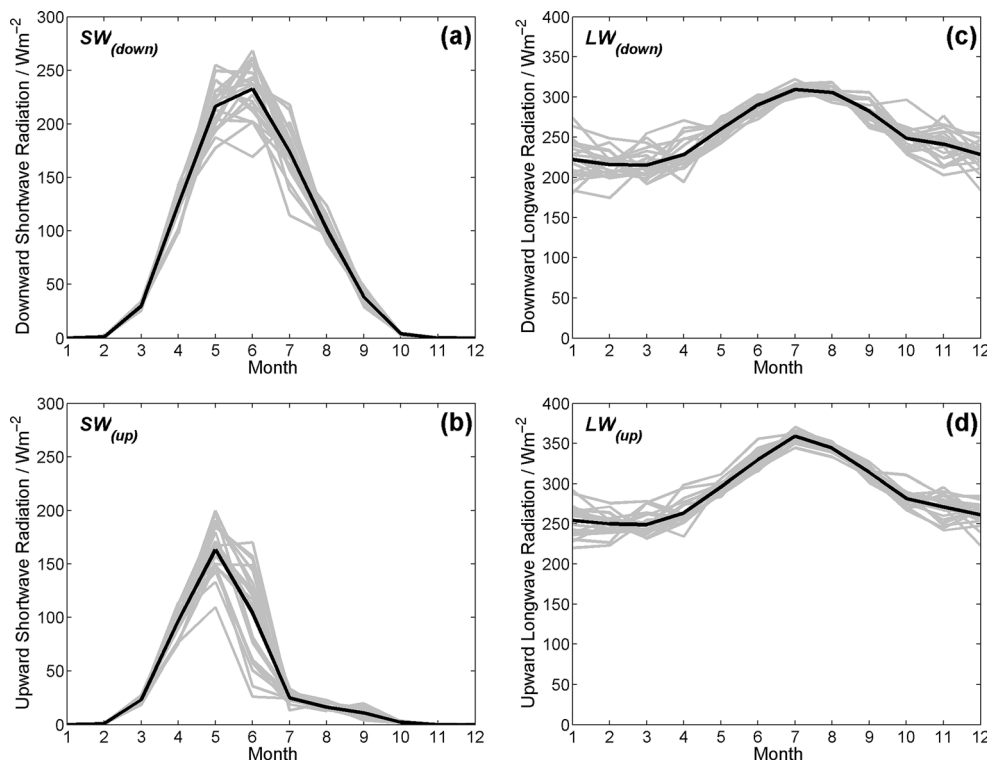
| Parameter | Instrument | Type | Manufacturer | Serial no. | WRMC no. |
|---|---------------|-------|--------------|------------|----------|
| LW _{down} LW _{up} | Pyrgeometer | PIR | Eppley | 28897 F3 | 11001 |
| | | PIR | Eppley | 28858 F3 | 11002 |
| | | PIR | Eppley | 28859 F3 | 11003 |
| | | PIR | Eppley | 28895 F3 | 11004 |
| SW _{down} SW _{up} Diffuse radiation | Pyranometer | CM11 | Kipp&Zonen | 913711 | 11009 |
| | | CM11 | Kipp&Zonen | 913704 | 11010 |
| | | CM11 | Kipp&Zonen | 913708 | 11011 |
| | | CM11 | Kipp&Zonen | 913707 | 11014 |
| | | CM11 | Kipp&Zonen | 913709 | 11015 |
| | | CM11 | Kipp&Zonen | 913712 | 11016 |
| | | CMP22 | Kipp&Zonen | 100216 | 11021 |
| | | CMP22 | Kipp&Zonen | 100217 | 11022 |
| | | CMP22 | Kipp&Zonen | 100219 | 11023 |
| Direct radiation | Pyrheliometer | NIP | Eppley | 28692 E6 | 11005 |
| | | NIP | Eppley | 28694 E6 | 11006 |
| | | NIP | Eppley | 28058 E6 | 13017 |
| | | | | | |

The individual attribution to the measurements is registered in the metadata of the electronic dataset <http://dx.doi.org/10.1594/PANGAEA.150000>

values that are based on hourly mean values similar to Maturilli et al. (2013). Seasonal mean values are then calculated from monthly means. Since there are only sporadic hours with clear-sky conditions in Ny-Ålesund that would not suffice for representative statistics, our analysis is based on measurements under all-sky conditions.

During the 21-year observation period, the monthly mean global shortwave radiation SW_{down} reveals large interannual variability during the summer months (Fig. 1). This variability is primarily caused by the different occurrence of clouds during the various sunlit seasons, as global shortwave radiation refers to all-sky conditions. Obviously, the amount of

Fig. 1 Ny-Ålesund monthly mean values (gray lines for all years of observation, black line for overall mean) for global shortwave radiation SW_{down} (a), reflected shortwave radiation SW_{up} (b), downward longwave radiation LW_{down} (c), and upward radiation LW_{up} (d), respectively



global shortwave radiation is the base for the reflected shortwave radiation that is modified by surface conditions. The largest variability in monthly mean reflected shortwave radiation is found in May and June, the months with the largest modification in surface texture due to the onset of the snow melt season. In the year 2006, the reflected shortwave radiation values have been much lower than in all other years, as shown by the lowermost gray line in Fig. 1b. In fact, an unusual warm period by the end of April 2006 (Maturilli et al. 2013) caused an unusual early onset of snow melt and consequent change of surface reflectivity.

While the upward longwave radiation LW_{up} depends on surface properties and temperature, the downward longwave radiation LW_{down} depends on atmospheric temperature and humidity, and is strongly influenced by the presence of clouds and the atmospheric water vapor content. Higher atmospheric temperatures in summer result in larger longwave radiation fluxes. Although the absolute values are smaller during the dark period, the interannual and month-to-month variability is much larger. Reasons for the strong longwave radiation variability in polar night conditions are both the large winter variability in atmospheric temperature and humidity (Maturilli et al. 2013), and the radiative effect of clouds.

The annual cycles of the shortwave, longwave, and net radiation budget are shown in Fig. 2, displaying the average monthly mean values over the 21-year observation period from 1 August 1992 to 31 July 2013. As indicated by the 1σ standard deviation, the largest interannual variability in net radiation budget Q_{net} is observed during the spring and summer season, related to the described variability in shortwave radiation during the snow melt season. Changes on a long term become apparent by analyzing the development of the radiation data over the 21-year observation period.

4 Long-term change in Ny-Ålesund surface radiation

Covering a period just about more than 20 years, the high-quality surface radiation measurements may not yet define climatic trends, but indicate tendencies related to Arctic climate change. In the following, the surface radiation measurements are presented in terms of their change over the period August 1992 to September 2013.

The annual mean net radiation budget for the complete years 1993 to 2012 is shown in Fig. 3. Surprisingly, the annual mean net radiation budget in Ny-Ålesund has positive values for more than a decade, with a total average of 5.3 Wm^{-2} . The linear regression of the annual mean values points towards a substantial increase of $+4.9 \pm 2.9 \text{ Wm}^{-2}$ per decade. Even if unlikely inhomogeneities of the measurements after the instrumental change from CM11 to CMP22 in August 2011 were considered, it should be noted that the total average of

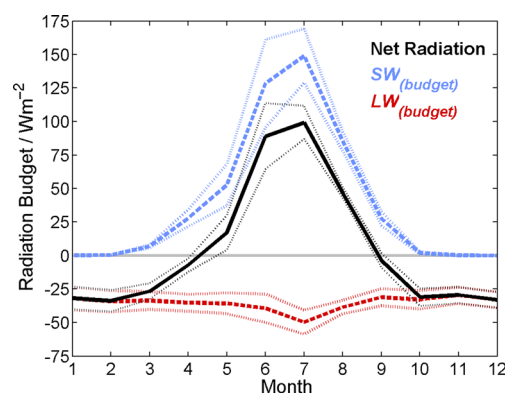


Fig. 2 Ny-Ålesund 21-year average monthly mean values of shortwave radiation budget $SW_{(budget)} = SW_{down} - SW_{up}$ (red dashed line), longwave radiation budget $LW_{(budget)} = LW_{down} - LW_{up}$ (blue dashed line), and net radiation budget $Q_{net} = SW_{(budget)} + LW_{(budget)}$ (black line), each $\pm 1\sigma$ standard deviation of monthly means (colored dotted lines, respectively)

the years 1993 to 2010 is 4.1 Wm^{-2} , while the linear regression in this shorter period gives $+4.2 \pm 3.2 \text{ Wm}^{-2}$ per decade.

Considering their contribution to the long-term change in annual mean net radiation budget, the shortwave and longwave radiation budget values are listed in Table 2. Looking at the annual mean, it appears as if changes in the shortwave radiation budget are solely responsible for the long-term increase in the net radiation budget.

Due to obliquity, the main shortwave and longwave radiation contributions to the net radiation budget strongly depend on the season. To identify the main reason for the increase of net radiation budget in Ny-Ålesund, the subsequent analyses refer to the standard meteorological seasons with spring (March, April, and May), summer (June, July, and August), autumn (September, October, and November), and winter (December of previous year, January, February), respectively. Figure 4 displays the seasonal mean net radiation budget for the observation period from August 1992 to September 2013. Evidently, there is a positive contribution to the net radiation budget increase throughout all seasons. By far, the largest increase is observed during the summer months, with $+8.4 \pm 8.2 \text{ Wm}^{-2}$ per decade. During the other seasons, the increase is smaller and not significant due to the large regression uncertainty: $+3.2 \pm 5.1 \text{ Wm}^{-2}$ per decade in spring, $+1.5 \pm 3.2 \text{ Wm}^{-2}$ per decade in autumn, and $+3.8 \pm 4.0 \text{ Wm}^{-2}$ per decade in winter. All seasonal and annual mean values of short- and longwave radiation parameters are summarized in Table 2.

In regard of the shortwave contribution to the net radiation budget, naturally the spring and summer seasons are the most affected. The seasonal mean of global and reflected shortwave radiation for spring and summer are shown in Fig. 5, respectively. Year-to-year variability is especially large in summer, with seasonal mean values of global shortwave radiation varying from 188.9 Wm^{-2} (2011) to 145.7 Wm^{-2} in 2013, when the summer has been unusually cloudy with weeks of fog and rain. Linear regression of the summer mean global

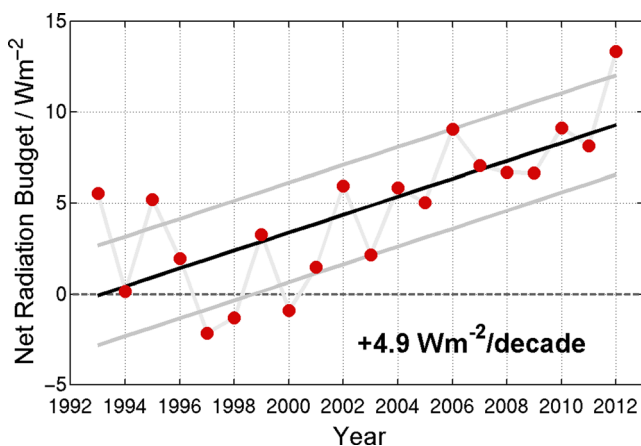


Fig. 3 Ny-Ålesund annual mean net radiation budget Q_{net} (red dots), with the linear regression (black line) and regression uncertainty (gray lines, respectively) indicating an increase of $+4.9 \pm 2.9 \text{ Wm}^{-2}$ per decade

shortwave radiation indicates a slight increase of $4.9 \pm 12.6 \text{ Wm}^{-2}$ per decade, with low relevance due to the large scatter of the data represented in the large regression uncertainty. More consistent is the observed decrease in springtime mean global shortwave radiation, given by linear regression as $-5.9 \pm 6.2 \text{ Wm}^{-2}$ per decade. Even with this decrease, the net shortwave radiation budget in spring is increasing, as the decrease in seasonal mean reflected shortwave radiation is even larger ($-9.5 \pm 7.8 \text{ Wm}^{-2}$ per decade). Also, the summer mean reflected shortwave radiation is decreasing (by $-7.0 \pm 13.9 \text{ Wm}^{-2}$ per decade), pronouncing the positive summer contribution to the increasing net radiation budget. Again, the large regression uncertainty implies low relevance of the described tendencies.

The main longwave contribution to the net radiation budget increase is illustrated in Fig. 6, showing the seasonal mean values of up- and downward longwave radiation for summer and winter. No relevant changes are found for the summer months, with a decrease of $-1.4 \pm 4.6 \text{ Wm}^{-2}$ per decade in downward longwave radiation and an increase of $2.2 \pm 5.1 \text{ Wm}^{-2}$ per decade in upward longwave radiation.

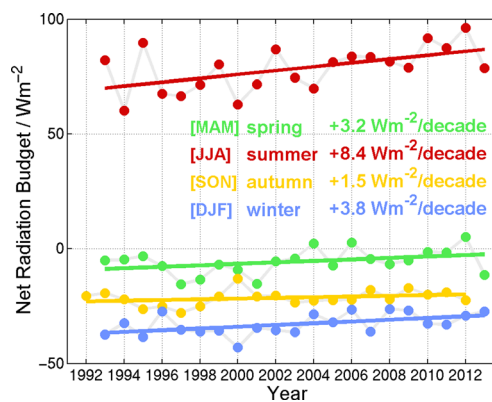


Fig. 4 Ny-Ålesund seasonal mean net radiation budget Q_{net} for spring (green dots), summer (red dots), autumn (yellow dots), and winter (blue dots), with the linear regression (colored lines, respectively). The according regression uncertainties are listed in Table 2

However, despite a large scatter of the data, a considerable increase in winter mean downward longwave radiation becomes obvious, amounting to $+15.6 \pm 11.6 \text{ Wm}^{-2}$ per decade. Not an independent parameter, this increase is partly due to the large increase observed in winter mean upward longwave radiation, amounting to $+11.6 \pm 10.9 \text{ Wm}^{-2}$ per decade. As the emission of longwave radiation by Earth and atmosphere is related to surface and air temperature, the strong increase in winter mean longwave radiation values is tied to changes in snow cover and an observed winter warming.

5 Changes in temperature and onset of snow melt

As documented in Maturilli et al. (2013), the annual mean temperature from 1994 to 2010 in Ny-Ålesund has been increasing by $+1.35 \text{ K}$ per decade. In August 2011, the meteorological tower has been shifted by 40 m and the data logging system has been renewed. Unfortunately, these changes brought along technical problems resulting in missing data for the 2-m temperature on up to 3 days per month between September 2011 and March 2012, as well as a continuous period without

Table 2 Observed long-term changes of various surface radiation parameters in Wm^{-2} per decade for the period 1 August 1992 to 1 September 2013, and of surface air temperature in K per decade for the period 1 August 1993 to 31 December 2013

| | Spring | Summer | Autumn | Winter | Annual mean |
|----------------------|----------------|-----------------|----------------|-----------------|----------------|
| SW_{down} | -5.9 ± 6.2 | 4.9 ± 12.6 | -0.7 ± 2.0 | – | 0.8 ± 3.6 |
| SW_{up} | -9.5 ± 7.8 | -7.0 ± 13.9 | -0.8 ± 1.4 | – | -4.1 ± 5.4 |
| LW_{down} | 1.9 ± 9.8 | -1.4 ± 4.6 | 4.5 ± 9.4 | 15.6 ± 11.6 | 5.4 ± 4.3 |
| LW_{up} | 2.2 ± 8.4 | 2.2 ± 5.2 | 3.1 ± 6.5 | 11.6 ± 10.9 | 5.4 ± 3.7 |
| Net Radiation Budget | 3.2 ± 5.1 | 8.4 ± 8.2 | 1.5 ± 3.2 | 3.8 ± 3.9 | 4.9 ± 2.9 |
| SW_{budget} | 3.5 ± 5.9 | 12.0 ± 12.0 | 0.1 ± 1.8 | – | 4.9 ± 4.0 |
| LW_{budget} | -0.2 ± 4.2 | -3.6 ± 5.3 | 1.4 ± 3.7 | 3.9 ± 3.9 | 0.0 ± 2.6 |
| Temperature | 0.7 ± 1.7 | 0.7 ± 0.5 | 0.8 ± 1.4 | 3.1 ± 2.4 | 1.3 ± 0.7 |

Values with exceeding regression uncertainty are marked as irrelevant by italic type

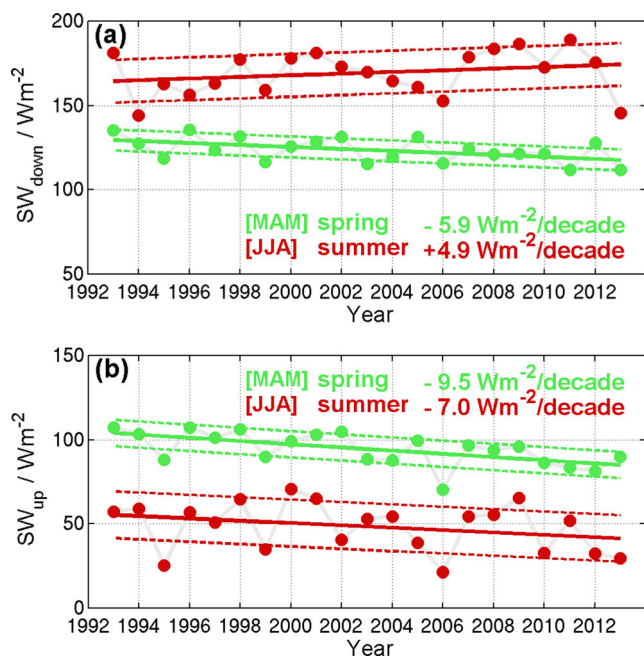


Fig. 5 Ny-Ålesund seasonal mean global and reflected shortwave radiation (a, b, respectively) for spring (green dots) and summer (red dots), with the linear regression (colored lines, respectively) and regression uncertainty (colored dashed lines, respectively)

data between 13 May and 8 June 2012. The seasonal average values presented here have thus been verified and checked for consistency with the temperature measured at 10-m height. The missing 2-m temperature data in May and June 2012 have been substituted with the according 10-m temperature value minus the long-term mean temperature difference between the two

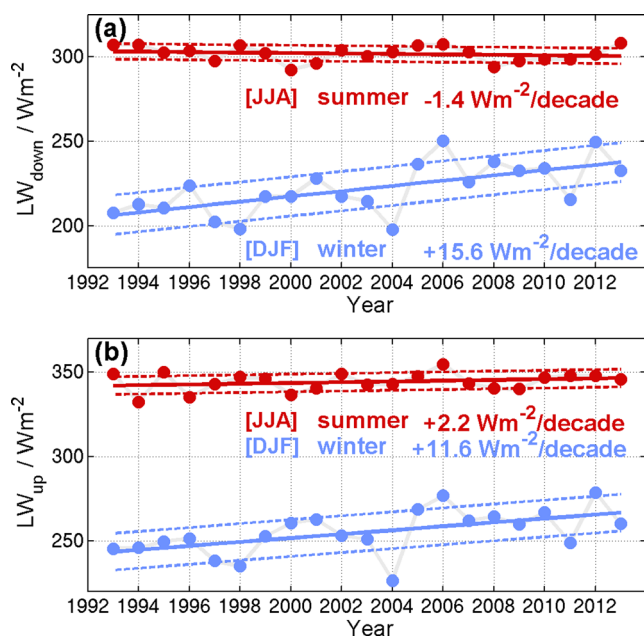


Fig. 6 Ny-Ålesund seasonal mean down- and upward longwave radiation (a, b, respectively) for summer (red dots) and winter (blue dots), with the linear regression (colored lines, respectively) and regression uncertainty (colored dashed lines, respectively)

altitude levels for the period May–June (0.3 K). A potential step in the dataset due to the relocation of the mast has been excluded by comparison with the temperature measurements that are simultaneously performed with synoptic observation time schedule by the Norwegian Meteorological Institute in Ny-Ålesund (data accessible via <http://eKlima.met.no>). Any changes have been found to be within the uncertainty limits of the instrumentation. Updating the observations presented in Maturilli et al. (2013), the annual mean temperature increase in Ny-Ålesund for the years 1994 to 2013 amounts to $+1.3 \pm 0.7$ K per decade.

The dimension of this observed warming gets even more impressive when separated to seasons as shown in Fig. 7, similar to the radiation data. Over the two decades, warming is observed in all seasons of the year. Regression uncertainties exceeding the actual temperature increase in spring ($+0.7 \pm 1.7$ K per decade) and autumn ($+0.8 \pm 1.4$ K per decade) limit the meaning of these values, while the temperature increase of $+0.7 \pm 0.5$ K per decade in the summer season is a more reliable contribution to the observed general warming. By far, the largest temperature increase is observed for the winter period. Despite its large variability, the seasonal mean temperature of the winter months increases by astonishing $+3.1 \pm 2.4$ K per decade. This winter warming is closely connected with the large increase in winter longwave radiation described above (Fig. 6). Overall, it can be concluded that the surface air temperature in Ny-Ålesund is increasing on a time scale of decades, and that by far the largest temperature increase occurs in the winter season.

Of course, the observed warming has an impact on the Ny-Ålesund environment. For example, the recent warm winters had several periods with precipitation in the form of rain rather than snow. As a consequence, in the following period with temperatures below the frost point, the surface has partly been covered by ice rather than snow. This difference in surface properties is apparent in the surface's reflection coefficient or albedo, which is defined as the ratio of reflected to global shortwave radiation. The dimensionless parameter varies between 0 for no reflection and 1 for perfect reflection of a white surface. The daily mean albedo values for the period beginning from March (Julian day 60) to mid of July (Julian day 200) are shown for all observation years from 1993 to 2013 in Fig. 8, respectively. High values around 0.8 indicate snow surface beneath the radiation sensor set-up. Thus, typically snow surface is identified until about end of May (Julian day <140). An obvious outlier is the spring of 2012, when albedo values of about 0.5 have been observed in March and April. In fact, this has been a year with a lot of rain precipitation during the winter months that resulted in a solid transparent ice layer on the surface in spring, impacting, e.g., the population dynamics of vertebrate herbivores (Hansen et al. 2013). In this case, the albedo jumped up to 0.8 only during short periods with snowfall on top of the ice layer.

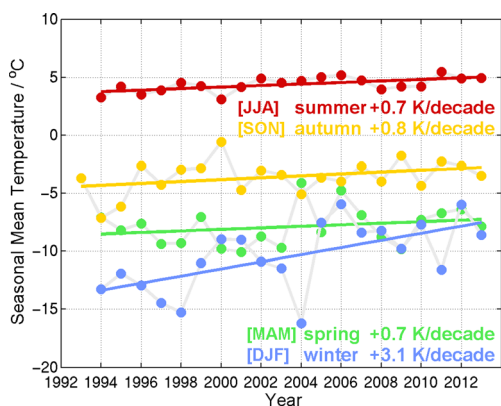


Fig. 7 Ny-Ålesund seasonal mean surface air temperature for spring (green dots), summer (red dots), autumn (yellow dots), and winter (blue dots), with the linear regression (colored lines, respectively). The corresponding regression uncertainties are listed in Table 2

Albedo values around 0.1 are typical for the uncovered tundra ground found beneath the radiation sensor set-up during the summer months, at latest from beginning of July (Julian day 182). The transition from high to low albedo values thus indicates the disappearance of the snow cover. It is a local measure that refers to the location of the radiation sensor set-up and may differ for other parts of the fjord surrounding. Yet, it is linked to the Ny-Ålesund temperature observations and indicates the onset of the snow melt season. From Fig. 8, it becomes evident that the date of snow cover disappearance varies over the years.

Considering the first day of the year with a daily mean albedo value smaller than 0.2 being the first day without snow cover, Fig. 9 shows the annual incidence of snow cover disappearance over the 21-year observation period. Determining the Julian date of the first snow-free day, linear regression indicates that the time of snow disappearance is shifting to an earlier date by -4.8 ± 8.3 days per decade. As snow disappearance commonly leads to a sharp transition in albedo, the chosen value is not critical and the overall picture changes only slightly for

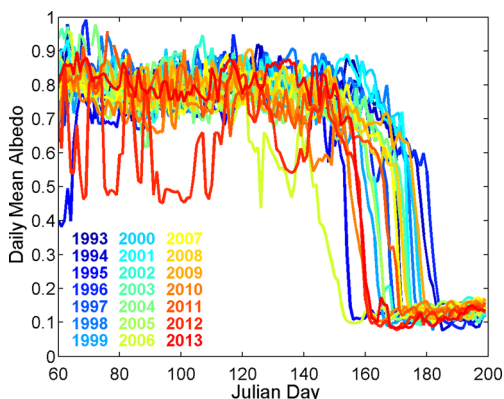


Fig. 8 Daily mean albedo SW_{down}/SW_{up} at the Ny-Ålesund BSRN radiation sensor set-up, on Julian days for all observation years from 1993 to 2013 (color-coded)

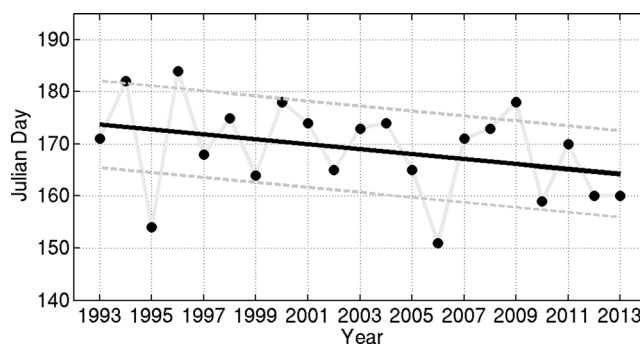


Fig. 9 First day of each year from 1993 to 2013 assumed to have a predominantly snow-free surface beneath the radiation sensor set-up because of a daily mean albedo <0.2 , in Julian days (black dots) with linear regression (black line) and regression uncertainty (gray lines)

other thresholds (e.g., -4.9 ± 8.4 days per decade for a daily mean albedo threshold of 0.3). Thus on average, versus the end of the 21-year observation period, the snow melt season starts about 1 week earlier than at the beginning.

Although this local albedo measure may not be used to infer the exact timing of the snow melt season in the Ny-Ålesund surrounding, the qualitative conclusion that the onset of snow melt has shifted to an earlier period of the year is valid due to the connection with the observed increase in temperature. Using temperature as a potential indicator for the snow cover free season, the first day after summer of each year from 1993 to 2013 with a daily mean temperature below the freezing point has shifted by $+9.0 \pm 11.2$ days per decade, postponing the cold season by more than 2 weeks over the 21-year observation period. The prolonged season above the freezing point and consequently shorter period of snow covered ground allows for changes in vegetation growth and related behavior of migratory birds (Buchwal et al. 2013; Kuhlmann Clausen and Clausen 2013).

6 Discussion

The observed changes of surface radiation and surface air temperature in Ny-Ålesund, Svalbard, over the last two decades, reveal regional climatic changes connected to global warming. While the annual mean surface air temperature has increased by $+1.3 \text{ K} \pm 0.7 \text{ K}$ per decade, the largest contribution to this warming accounts for the winter season, featuring a mean seasonal temperature increase of $+3.1 \pm 2.4 \text{ K}$ per decade. During recent years, the higher temperature lead to winter periods with rain rather than snow, modifying the snow cover of the landscape. From the Earth's heat balance perspective, snow on the ground has an influence both on the surface albedo and on the terrestrial radiation. Due to the complexity of the coupled Earth-atmosphere system involving global and regional feedback processes, it exceeds the scope of this manuscript to identify the causes leading to the

observed long-term changes in surface radiation. However, some potentially contributing factors are discussed below.

Concerning the longwave radiation, the snow cover acts as isolation to the ground and suppresses the upwelling longwave radiation while the open ground may emit longwave radiation to a larger part. Along with the corresponding increase in winter surface air temperature, our observations show a mean winter increase both for down- and upward longwave radiation. The winter net longwave radiation balance is mainly affected by processes in the atmospheric column. The downward longwave radiation varies with increasing CO₂ and other greenhouse gases, with atmospheric humidity, and with cloud cover. In Arctic winter, clouds have a net warming effect on the surface with their dominant radiative effect acting on the longwave radiative fluxes (Curry et al. 1996). The longwave cloud forcing is a function of cloud temperature, height and microphysics, with liquid clouds being the significant factor in the overall positive cloud forcing (Shupe and Intrieri 2004). Thus in terms of contributing to the Ny-Ålesund surface radiation balance, long-term changes in cloud cover have to be considered to potentially occur in quantity, in vertical distribution, or microphysical state of the cloud particles. Considering the cloud cover over Ny-Ålesund, the available long-term ceilometer measurements of the cloud base are affected by instrumental changes, and moreover do not provide information about the spatial dimension of the clouds as they refer to the vertical column above the instrument. Satellite observations may have the advantage of horizontal resolution, but both passive and active satellite instruments have difficulties in Arctic cloud retrieval especially during winter (Zygmuntowska et al. 2012). Also, common atmospheric reanalyses and global climate models suffer from considerable biases in regard to radiative fluxes and cloud fraction (Walsh et al. 2009; Zib et al. 2012; Zygmuntowska et al. 2012; Wild et al. 2013).

Being a natural greenhouse gas, also water vapor affects the atmospheric longwave emission. Surface atmospheric humidity observations in Ny-Ålesund indicate a slight increase in annual mean water vapor mixing ratio since 1993 (Maturilli et al. 2013) that may be related to more intense local evaporation due to changes in snow cover as well as to episodic augmentation of humidity related to cyclonic systems. Intense filamentary moisture intrusion events are a common feature in the Arctic and can induce large episodic increases of downward longwave radiation along the pole-ward moving branch of cyclones (Doyle et al. 2011; Woods et al. 2013). As one of the main sectors for humidity intrusions towards the Arctic is the Atlantic sector (Woods et al. 2013), the long-term observations at Svalbard may substantially differ from other regions in the Arctic due to the location relative to the Atlantic cyclone tracks. In general, the number of cyclones entering the Arctic has increased, especially for the winter season (Sepp and Jaagus 2011).

Increasing levels of CO₂ and other greenhouse gases have to be considered, but their radiative impact is effective throughout all seasons rather than having a maximum during polar night. Also, aerosols may impact Arctic climate by perturbing the radiative balance via direct and indirect aerosol effects (Curry et al. 1996). In Ny-Ålesund, photometer measurements have shown low background values of tropospheric aerosol optical depth for all seasons, with occasional Arctic haze events occurring in springtime (Herber et al. 2002). Another parameter potentially influencing the winter downward longwave radiation are thermal inversions in the vertical temperature profile (Bintanja et al. 2011) that are frequently observed in the planetary boundary layer above Ny-Ålesund.

Overall, the interactions of aerosol, clouds, water vapor, and other greenhouse gases as well as their feedback processes involving longwave radiative fluxes in the Arctic polar night have a high complexity. Based on the currently available observation data, it is not possible to identify the main contribution to the wintertime longwave radiation and surface air temperature increase observed in Ny-Ålesund. The presented climatology and time series of high-quality surface radiation data provide an observational fragment of the complex radiative feedback processes in the Arctic.

The observed warming over the last two decades in Ny-Ålesund also impacts other parts of the radiation budget, and has induced changes of the Svalbard environment. For the spring and summer months, a considerable decrease in reflected shortwave radiation is found for the observation period due to changes in surface reflectivity, being the main contribution to the observed increase in annual mean net radiation budget. The surface albedo changes drastically with the onset of snow melt, and this step from snow covered to open tundra surface has occurred earlier by about 1 week over the 20-year observation period. Considering that the first day after summer with daily mean temperature below the freezing point has shifted by more than 2 weeks towards a later date, this sums up to a warm season prolonged by about 3 weeks compared to the beginning of the observations. As the tundra shows a distinctively mild climate during the snow-free season when the terrestrial ecology is most active (Ohmura 2000), the prolongation of the warm season's duration has a strong impact on the Svalbard tundra ecosystem.

Acknowledgments Many thanks are expressed to the station personnel of the AWIPEV research base (former Koldewey station) in Ny-Ålesund for their contribution to maintain the instrumentation hardware and software infrastructure. We thank in particular B. Loose for planning, erecting, and updating the measurement site, J. Graeser for technical maintenance of the instrumentation, and S. Debatin for data handling.

Open Access This article is distributed under the terms of the Creative Commons Attribution License which permits any use, distribution, and

reproduction in any medium, provided the original author(s) and the source are credited.

References

- Bintanja R, Graverson RG, Hazeleger W (2011) Arctic winter warming amplified by the thermal inversion and consequent low infrared cooling to space. *Nat Geosci* 4:758–761. doi:10.1038/NNGEO1285
- Buchwal A, Rachlewicz G, Fonti P, Cherubini P, Gärtner H (2013) Temperature modulates intra-plant growth of *Salix Polaris* from a high Arctic site (Svalbard). *Polar Biol* 36:1305–1318. doi:10.1007/s00300-013-1349-x
- Cavalieri DJ, Parkinson CL (2012) Arctic sea ice variability and trends, 1979–2010. *Cryosphere* 6:881–889. doi:10.5194/tc-6-881-2012
- Curry JA, Rossow WB, Randall D, Schramm JL (1996) Overview of Arctic cloud and radiation characteristics. *J Clim* 9:1731–1764. doi:10.1175/1520-0442(1996)09<1731:OOACAR>2.0.CO;2
- Curry JA, Schramm J, Ebert EE (1995) On the sea ice albedo climate feedback mechanism. *J Clim* 8:240–247. doi:10.1175/1520-0442(1995)08<0240:SIACFM>2.0.CO;2
- Dessler AE, Schoeberl MR, Wang T, Davis SM, Rosenlof KH (2013) Stratospheric water vapor feedback. *PNAS* 110:18087–18091. doi:10.1073/pnas.1310344110
- Doyle JG, Lesins G, Thackray CP, Perro C, Nott GJ, Duck TJ, Damoah R, Drummond JR (2011) Water vapor intrusions into the high Arctic during winter. *Geophys Res Lett* 38, L12806. doi:10.1029/2011GL047493
- Dutton EG, Nelson DW, Stone RS, Longenecker D, Carbaugh G, Harris JM, Wendell J (2006) Decadal variations in surface solar irradiance as observed in a globally remote network. *J Geophys Res* 111, D19101. doi:10.1029/2005JD006901
- Francis JA, Chan W, Leathers DJ, Miller JR, Veron DE (2009) Winter northern hemisphere weather patterns remember summer Arctic sea-ice extent. *Geophys Res Lett* 36, L07503. doi:10.1029/2009GL037274
- Francis JA, Hunter E (2007) Changes in the fabrics of the Arctic's greenhouse blanket. *Environ Res Lett* 2:045011. doi:10.1088/1748-9326/2/4/045011
- Garcia RR, Randel WJ (2008) Acceleration of the Brewer–Dobson circulation due to increases in greenhouse gases. *J Atmos Sci* 65:2731–2739. doi:10.1175/2008JAS2712.1
- Graverson RG, Mauritsen T, Tjernström M, Källén E, Svensson G (2008) Vertical structure of recent Arctic warming. *Nature* 451:53–56. doi:10.1038/nature06502
- Hansen BB, Grøtan V, Aanes R, Sæther BE, Stien A, Fuglei E, Ims RA, Yoccoz NG, Pedersen ÅØ (2013) Climate events synchronize the dynamics of a resident vertebrate community in the high Arctic. *Science* 339:313–315. doi:10.1126/science.1226766
- Herber A, Thomason LW, Gernandt H, Leiterer U, Nagel D, Schulz KH, Kaptur J, Albrecht T, Notholt J (2002) Continuous day and night aerosol optical depth observations in the Arctic between 1991 and 1999. *J Geophys Res* 107:4097. doi:10.1029/2001JD000536
- Intergovernmental Panel on Climate Change (2007) In: Solomon S, Qin D, Manning M, Chen Z, Marquis M, Averyt KB, Tignor M, Miller HL (eds) *Climate Change 2007: The Physical Science Basis*. Cambridge Univ Press, New York
- Intergovernmental Panel on Climate Change (2013) Summary for Policymakers. In: Stocker TF, Qin D, Plattner GK, Tignor M, Allen SK, Boschung J, Nauels A, Xia Y, Bex V, Midgley PM (eds) *Climate Change 2013: The Physical Science Basis. Contribution of Working Group I to the Fifth Assessment Report of the Intergovernmental Panel on Climate Change*. Cambridge Univ Press, Cambridge
- Kuhlmann Clausen K, Clausen P (2013) Earlier Arctic springs cause phenological mismatch in long-distance migrants. *Oecologia* 173:1101–1112. doi:10.1007/s00442-013-2681-0
- Kupfer H, Herber A, König-Langlo G (2006) Radiation Measurements and Synoptic Observations at Ny-Alesund, Svalbard. Reports on Polar Research 538. Alfred Wegener Institute for Polar and Marine Research, Bremerhaven, hdl:10013/epic.10543.d001
- König-Langlo G, Sieger R, Schmithüsen H, Bücken A, Richter F, Dutton EG (2013) Baseline Surface Radiation Network (BSRN), Update of the Technical Plan for BSRN Data Management. GCOS-174, WCRP/WMO, www.wmo.int/pages/prog/gcos/Publications/gcos-174.pdf
- Lanconelli C, Busetto M, Dutton EG, König-Langlo G, Maturilli M, Sieger R, Vitale V, Yamanouchi T (2011) Polar baseline surface radiation measurements during the International Polar Year 2007–2009. *Earth Syst Sci Data* 3:1–8. doi:10.5194/essd-3-1-2011
- Lindsay R, Zhang J (2005) The thinning of the Arctic sea ice, 1988–2003. Have we passed a tipping point? *J Clim* 18:4879–4894. doi:10.1175/JCLI3587.1
- Maturilli M, Herber A, König-Langlo G (2013) Climatology and time series of surface meteorology in Ny-Ålesund, Svalbard. *Earth Syst Sci Data* 5:155–163. doi:10.5194/essd-5-155-2013
- McArthur LJB (2005) Baseline Surface Radiation Network (BSRN), Operations Manual Version 2.1. WMO/TD-No.1274, WCRP/WMO. www.wmo.int/pages/prog/gcos/documents/gruanmanuals/WCRP/WCRP21_TD1274_BSRN.pdf
- Ohmura A (2000) Climate on tundra and thoughts on causes of regional climate differences. *Annals of Glaciology* 31:10–14.
- Ohmura A, Dutton EG, Forgan B, Fröhlich C, Gilgen H, Hegner H, (1998) Baseline Surface Radiation Network (BSRN/WCRP): new precision radiometry for climate research. *BAMS* 79: 2115–2136
- Overland JE, Wang M (2010) Large-scale atmospheric circulation changes are associated with the recent loss of Arctic sea ice. *Tellus* 62A:1–9. doi:10.1111/j.1600-0870.2009.00421.x
- Screen JA, Simmonds I (2010) The central role of diminishing sea ice in recent Arctic temperature amplification. *Nature* 464:1334–1337. doi:10.1038/nature09051
- Sepp M, Jaagus J (2011) Changes in the activity and tracks of Arctic cyclones. *Clim Chang* 105:577–595. doi:10.1007/s10584-010-9893-7
- Shupe MD, Intrieri J (2004) Cloud radiative forcing of the Arctic surface: the influence of cloud properties, surface albedo, and solar zenith angle. *J Clim* 17:616–628. doi:10.1175/1520-0442(2004)017<0616:CRFOTA>2.0.CO;2
- Walsh JE, Chapman WL, Portis DH (2009) Arctic cloud fraction and radiative fluxes in atmospheric reanalyses. *J Clim* 22:2316–2334. doi:10.1175/2008JCLI2213.1
- Wild M, Folini D, Schär C, Loeb N, Dutton EG, König-Langlo G (2013) The global energy balance from a surface perspective. *Clim Dyn* 40:3107–3134. doi:10.1007/s00382-012-1569-8
- Woods C, Caballero R, Svensson G (2013) Large-scale circulation associated with moisture intrusions into the Arctic during winter. *Geophys Res Lett* 40:4717–4721. doi:10.1002/grl.50912
- Zhang X, Sorteberg A, Zhang J, Gerdes R, Comiso JC (2008) Recent radical shifts of atmospheric circulations and rapid changes in Arctic climate system. *Geophys Res Lett* 35, L22701. doi:10.1029/2008GL035607
- Zib B, Dong X, Xi B, Kennedy A (2012) Evaluation and intercomparison of cloud fraction and radiative fluxes in recent reanalyses over the Arctic using BSRN surface observations. *J Clim* 25:2291–2305. doi:10.1175/JCLI-D-11-00147.1
- Zygmuntowska M, Mauritsen T, Quaas J, Kaleschke L (2012) Arctic clouds and surface radiation—a critical comparison of satellite retrievals and the ERA-interim reanalysis. *Atmos Chem Phys* 12:6667–6677. doi:10.5194/acp-12-6667-2012